NON-METAL DIFFUSIVITY IN SOME BINARY TRANSITION METAL NITRIDES AND CARBIDES

D. Rafaja[1] and W. Lengauer[2]

[1]*Faculty of Mathematics and Physics, Charles University, 121 16 Praha 2, Ke Karlovu 5, Czech Republic*
[2]*Institute for Chemical Technology of Inorganic Materials, Vienna University of Technology, Getreidemarkt 9, A-1060 Vienna, Austria*

Abstract

Two methods, which are used for calculation of diffusion coefficients in multiphase binary systems are outlined and compared – the investigation of the layer growth kinetics and the fitting of concentration profiles. The methods are discussed in view of their particular advantages and disadvantages and illustrated on the non-metal diffusion coefficients in the Nb-N, Nb-C, Cr-N, Cr-C, Ta-N and Ta-C systems. It is shown that the best way for determining the non-metal diffusivity in multiphase systems is the combined refinement of diffusion coefficients employing both the layer growth enhancement and the concentration profile fitting.

1 Introduction

The transition metal nitrides and carbides are hard refractory materials, which are advantageously used as diffusion barriers, as construction materials for high-temperature applications, and in the production of cutting tools. In these compounds, diffusion processes occur both in production and use, and therefore the knowledge of diffusion kinetics is important. In addition, the diffusion couple experiments can offer an exceptional opportunity to obtain an insight into binary systems because the phase band structure arising during the diffusion processes represents an isothermal cut in the phase diagram. Still, the diffusion coefficients, which characterise the diffusion kinetics, are lacking in the majority of the nitrides and carbides of transition metals.

In principle, chemical diffusion experiments can be carried out as single-phase or multi-phase diffusion experiments. In the first case the in- or out-diffusion of the non-metal occurs in a single phase and only intraphase boundaries are observed. In the second case, several solid phases are formed and also interphase boundaries occur. Of course, the layout of the diffusion experiment determines the starting and boundary conditions upon the mathematical description of the diffusion process. For the starting and boundary conditions is not important how many phases are present in the diffusion couple or if the non-metal diffuses from a solid phase or from gas, but how the starting composition profile in the diffusion couple looks like and if the source of the in-diffusing non-metal is limited or not. As the nitrides and carbides of transition metals were prepared through diffusion of nitrogen from N_2 or carbon from graphite into pure metal in our most experiments, we will pay attention to the reactive diffusion assuming a non-limited source of the non-metal.

As the diffusivities of both nitrogen and carbon are much higher than the diffusivity of the metal in the majority of nitrides and carbides of transition metals, the diffusion process is usually regarded as a diffusion of the non-metal in a rigid metal grid. The positions of the metal atoms are assumed to be fixed, and the diffusion process is used to be described as the sole non-metal diffusion.

2 Model of the reactive diffusion

If samples of the pure metal are annealed in the nitrogen atmosphere or in the graphite powder, the reactive diffusion is described by the following model. At the beginning of the diffusion process all phases according to the phase diagram arise, starting from the non-metal-richest which is located at the sample surface, and ending with the non-metal-poor one which fills the core. During the diffusion process the concentration of the in-diffusing non-metal increases that can be observed as weight gain, as growth of the individual phases (the layer growth or the phase boundary movement) or as the change in the concentration profile. The layer growth in multiphase diffusion couples is known from experiments to follow the parabolic rule [1, 2]:

$$x_i = K_i\sqrt{t} \tag{1}$$

where x_i is the thickness of the phase (layer) i after the diffusion time t. K_i is the respective rate constant. By using the first and the second one-dimensional Fick's laws,

$$J = -D\frac{\partial c}{\partial x} \tag{2}$$

and

$$\frac{\partial c}{\partial t} = \frac{\partial}{\partial x}\left(D\frac{\partial c}{\partial x}\right) \tag{3}$$

and the one-dimensional continuity equation

$$\frac{\partial c}{\partial t} = -\frac{\partial J}{\partial x}, \tag{4}$$

equation (1) was approved theoretically by Kidson [3] to be valid for infinite (very thick) diffusion couples.

In Eqs. (2)-(4), J is the diffusion flow, D the diffusion coefficient and c the concentration of the non-metal. Kidson's analysis [3] also explained the meaning of the rate constant K, as the movement of phase boundaries was described by the following system of transcendental equations:

$$x_i = \left[\frac{D_i \left(c_i^+ - c_i^-\right)}{\Delta c_i} \times \frac{\exp\left(-\frac{\xi_i^2}{D_i}\right)}{\int_{\xi_{i-1}}^{\xi_i} \exp\left(-\frac{y'^2}{D_i}\right) dy'} - \frac{D_{i+1}\left(c_{i+1}^+ - c_{i+1}^-\right)}{\Delta c_i} \times \frac{\exp\left(-\frac{\xi_i^2}{D_{i+1}}\right)}{\int_{\xi_i}^{\xi_{i+1}} \exp\left(-\frac{y'^2}{D_{i+1}}\right) dy'} \right] \sqrt{t} \quad (5)$$

for the positions of the *(n-1)* outer phase boundaries and by

$$x_n = \left[\frac{D_n \left(c_n^+ - c_n^-\right)}{\Delta c_n} \times \frac{\exp\left(-\frac{\xi_n^2}{D_n}\right)}{\int_{\xi_{n-1}}^{\xi_n} \exp\left(-\frac{y'^2}{D_n}\right) dy'} - \frac{D_{n+1}\left(c_{n+1}^+ - c_{n+1}^-\right)}{\Delta c_n} \times \frac{\exp\left(-\frac{\xi_n^2}{D_{n+1}}\right)}{\int_{\xi_n}^{\infty} \exp\left(-\frac{y'^2}{D_{n+1}}\right) dy'} \right] \sqrt{t} \quad (6)$$

for the innermost (n-th) phase boundary. The symbols x_i and ξ_i denote the positions of phase boundaries in Cartesian co-ordinates and in the Boltzmann-Matano variables ($\xi = x/(2\sqrt{t})$, respectively; D_i is the non-metal diffusion coefficient in the i-th phase, $c_i{}^+$ and $c_i{}^-$ are the maximum and minimum concentrations within the phase i; Δc_i is the concentration jump at the i-th phase boundary (i.e. the width of the respective two-phase region in the phase diagram). The terms in the square brackets have the meaning of the rate constants K. A similar approach has been applied for finite diffusion couples taking into account that the non-metal diffuses through both surfaces [4]. This calculation yielded the same system of transcendental equations for the outer phases (5) and a modified equation for the last phase boundary:

$$x_n = \left[\frac{D_n \left(c_n^+ - c_n^-\right)}{\Delta c_n} \times \frac{\exp\left(-\frac{\xi_n^2}{D_n}\right)}{\int_{\xi_{n-1}}^{\xi_n} \exp\left(-\frac{y'^2}{D_n}\right) dy'} - \frac{D_{n+1}\left(c_{n+1}^+ - c_{n+1}^-\right)}{\Delta c_n} \times \frac{\exp\left(-\frac{\xi_n^2}{D_{n+1}}\right)}{\int_{\xi_n}^{\infty} \exp\left(-\frac{y'^2}{D_{n+1}}\right) dy'} \right] \sqrt{t} + \frac{D_{n+1}\left(c_{n+1}^+ - c_{n+1}^-\right)}{\Delta c_n} \times \frac{\exp\left(-\frac{\xi_n^2}{D_{n+1}}\right)}{\int_{\xi_n}^{\infty} \exp\left(-\frac{y'^2}{D_{n+1}}\right) dy'} \times \ell \int_{\ell/\sqrt{t}}^{\infty} \frac{1}{\tau^2} \exp\left(\frac{\xi_n \tau}{D_{n+1}}\right) \exp\left(\frac{-\tau^2}{4D_{n+1}}\right) d\tau \quad (7)$$

The additional term in Eq. (7) is a consequence of the finite sample geometry. In this case, the simplified equation of the layer growth contains rate constant, which depends on both the diffusion time and the sample thickness:

$$x_i = K_i(t, \ell)\sqrt{t} \quad (8)$$

Varying the diffusion time or the sample thickness, sufficent number of equations are obtained for the calculation of the diffusion coefficients in all phases. In practical applications, the finite sample geometry causes a layer growth enhancement against the parabolic law. Particularly, a broadening of the layer thickness is observed with decreasing sample thickness [5]. The analytical solution (Eq. 5 and 7) was proved by comparing the calculated layer growth with the layer growth simulated using the forward finite difference (FFD) method [6].

During the diffusion process also the concentration profile changes. At the beginning of the diffusion process the composition profile is characterised by a concentration sink having the maximum non-metal concentration at the sample surface and the zero non-metal concentration inside. After the diffusion time t, the concentration profile within individual phases can be approximated by:

$$c(y) = \left(c^+ - c^-\right) \frac{\int_{y(0)}^{y} \frac{1}{D(y')} \exp\left(-\int_{y(0)}^{y'} \frac{2y''dy''}{D(y'')}\right) dy'}{\int_{y(0)}^{y(\xi)} \frac{1}{D(y')} \exp\left(-\int_{y(0)}^{y'} \frac{2y''dy''}{D(y'')}\right) dy'} + c^+ \quad (9)$$

which is the result of the analytical solution of the second Fick's law (3), see [7], for example. y is the time-dependent Boltzmann-Matano variable ($y = x/(2\sqrt{t})$), D the diffusion coefficient, c^- the minimum and c^+ the maximum concentration within the phase being investigated. For the concentration-independent diffusion coefficient, the equation describing the concentration profile takes the simple form of the error function [1, 7].

3 Calculation of diffusion coefficients

3.1 Layer growth

Upon solving the system of transcendental equations (5, 6) the positions of phase boundaries can be calculated if the homogeneity ranges (c^+ and c^-) and the diffusion coefficients are known for all phases. On the contrary, the observed layer growth cannot be used to calculate diffusion coefficients, because the system of Eqs. (5) and (6) consists of n equations (for n known positions of phase boundaries) but it contains $n+1$ unknown diffusion coefficients. In addition, as the rate constants in Eq. (1) do not depend on the diffusion time, it is impossible to obtain the complete set of diffusion coefficients (the diffusion coefficients in all phases) from a

series of diffusion experiments carried out with different diffusion times. This has first been stated by Jost [1], who already reported several approaches, which should overcome this difficulty.

If one diffusion coefficient is known, the system of n transcendental equations (5) and (6) is sufficient for calculation of the n unknown remaining diffusion coefficients. However, this requirement is very restrictive when the diffusion coefficients are not accessible by using other methods. Another approach neglects the diffusion flow in the core. Thus, the diffusion coefficient for the non-metal in the core is not involved in the calculation of layer growth, and consequently the modified system of equations based on (5) and (6) is suitable for calculation of the n remaining diffusion coefficients [1]. This approximation can, however, be applied only if the concentration profile in the core is very flat, i.e. if its gradient is nearly equal to zero. This is the case if the solubility of non-metal in the metal is very low or if the diffusion experiment is started with a homogeneous sample containing only the solid solution of non-metal in the host metal that possesses the highest non-metal concentration. Then, the concentration profile in the core is completely flat, the concentration gradient is equal to zero and therefore the diffusion flow is negligible despite the finite diffusivity of the non-metal in the core.

3.2 Layer growth enhancement

Our procedure for calculating the non-metal diffusion coefficients from layer growth employs the layer growth enhancement and the successive disappearance of individual phases in wedge-shaped samples (Fig. 1). Such a sample geometry is favourable because the wedge contains apparently more samples with different thicknesses, which are annealed in the same experimental run (with exactly the same experimental conditions). If the angle of the wedge is sufficiently small (10°–15°), the wedge can still be regarded as a one-dimensional diffusion couple. This was verified experimentally by annealing wedge-shaped samples together with the planar diffusion couples having different thicknesses. The observed positions of phase boundaries were the same both in the wedges and in the parallel sheets.

The computing routine [8] used for calculation of diffusion coefficients simulates first the positions of phase boundaries for a single sample thickness and a certain diffusion time. Typically, a large sample thickness is used, at which all phases which are stable at the given temperature are still present in the sample. The calculus needs the maximum and the minimum concentrations in individual phases and the diffusion coefficient in the core as the input data. The limit concentrations must be known precisely, whereas the estimate of the diffusion coefficient in the core is sufficient. In the first computation step, the diffusion coefficients in outer phases are calculated. In the second step, the complete phase band

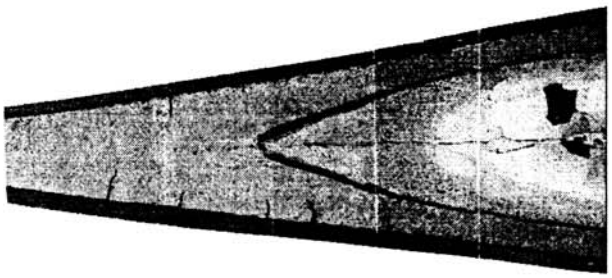

Figure 1: An example of the layer growth enhancement in wedge-shaped diffusion couples (Ta-C). The finite sample geometry accelerates the in-diffusion of non-metal, which can be observed as a deviation from the parabolic layer growth or as the layer growth enhancement in wedge-shaped specimens.

structure, i.e. the positions of the phase boundaries at different sample thicknesses, are simulated with the diffusion coefficients calculated in outer phases and with the estimated diffusion coefficient in the core. If the estimate of the diffusion coefficient in the core is lower than its correct value, the calculated layer growth enhancement is smaller than the measured one and vice versa. Thus the diffusion coefficient in the core can be refined by repeating this procedure until the differences between the calculated and the observed positions of phase boundaries drop below a desired limit.

3.3 Concentration profile fitting

Upon the concentration profile fitting, the diffusion coefficient in a single phase can be calculated by fitting the function (9) on the measured concentration profile. The diffusion coefficient can either be assumed to be independent of the non-metal concentration, $D \neq D(c)$, or to be a function of the non-metal concentration, $D = D(c)$. The calculation of the concentration profiles with the concentration-dependent diffusion coefficients according Eq. (9) must be performed iteratively. First, a starting concentration profile is calculated with a concentration-independent diffusion coefficient. The starting concentration profile is then used for calculation of the spatial distribution of the diffusion coefficient, $D = D(c(y))$. This is only possible if the relationship between the diffusion coefficient and the non-metal concentration is known. Regarding the experimental errors in the concentration profile measurement and the numerical stability of the solution, it is impossible to obtain a general form of the function describing the concentration dependence of the diffusion coefficient from the concentration profile fitting. Therefore, the concentration dependence of the diffusion coefficient is usually characterised by an analytical function, which parameters are refined. The following

exponential function has been established [9]:

$$D(c) = D_0 \exp\left[a\left(c^+ - c\right)\right] \qquad (10)$$

which has two free parameters, D_0 and a. c^+ means the highest non-metal concentration in the respective phase. More general concentration dependence of the diffusion coefficient can be obtained if the measured concentration profile is approximated "per partes" by the function (9) assuming a concentration-independent diffusion coefficient in each particular window. However, this approach works only with perfect concentration profiles.

Regarding the Arrhenius dependence of diffusivity and Eq. (10), the temperature and concentration dependence of the non-metal diffusion coefficient can be characterised by the function:

$$D(T, c) = D_0 \exp\left(-\frac{E}{k_B T}\right) \exp\left[a\left(c^+ - c\right)\right] \qquad (11)$$

which describes a two-dimensional surface in the semi-logarithmic representation of the diffusion coefficient.

4 Survey on the non-metal diffusion coefficients

Results presented in this section were obtained by using the combined refinement of diffusion coefficients if the quality of measured concentration profiles was sufficient. This approach yielded the concentration-independent diffusion coefficients (calculated from the layer growth enhancement in wedge-shaped samples) and the concentration-dependent diffusion coefficients (calculated from the concentration profiles). The investigation of the layer growth enhancement yielded diffusion coefficients in all phases which were present in the diffusion couple, whereas the concentration profiles were suitable only for calculation of diffusion coefficients in the non-metal-rich phases. Whenever both methods could be applied, the diffusion coefficients were compared. As these methods are independent, their combination offered a better insight into the diffusion kinetics because the concentration-dependent diffusion coefficients can be assigned to a certain non-metal concentration, whereas the concentration-independent diffusion coefficients correspond to the average non-metal concentration in the respective phase.

4.1 Nb-N system

The Nb-N system was investigated between 1400°C and 1800°C [10]. In this temperature region three phases are stable: the solid solution of nitrogen in niobium, α-Nb(N), having the space group Im3m and two nitride phases, β-Nb_2N ($P\bar{3}1m$) and δ-NbN (Fm3m). The homogeneity ranges measured using the electron probe microanalysis (EPMA/WDS) [11] are shown as a part of the phase diagram in Fig. 2. As the position of the nitrogen-rich boundary in the phase diagram (the maximum concentration) for the δ-NbN_{1-x} phase depends strongly on the nitrogen pressure, a different nitrogen pressure was applied at different temperatures to keep the nitrogen concentration at the sample surface constant. The diffusion coefficients obtained from layer growth for α-Nb(N), β-Nb_2N and δ-NbN are summarised in Fig. 3 (open symbols) and compared with the diffusion coefficients calculated from the nitrogen concentration profiles in δ-NbN_{1-x} (solid circles). The Arrhenius dependence of the diffusion coefficients yielded the activation energies and pre-exponential factors, which are given in Tab. 1. Comparable activation energies have been published in [12] for the temperature range 1100°C–1900°C as a result of the layer growth study: E (δ-NbN) = (3.31±0.26) eV and E (β-Nb_2N) = (3.35±0.40) eV.

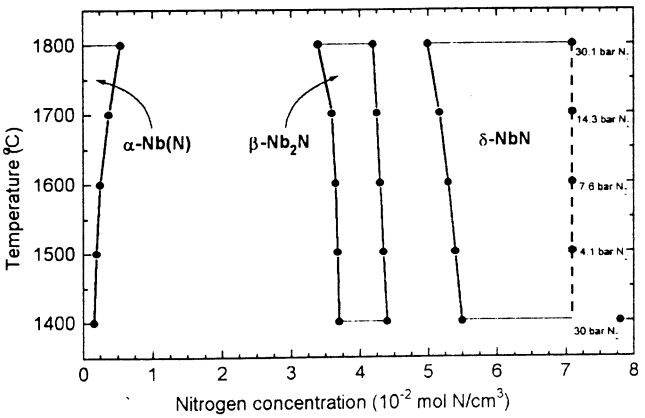

Figure 2: A part of the phase diagram for the Nb-N system. The circles indicate the limit concentrations used for calculation of diffusion coefficients from layer growth.

Table 1: Activation energies and pre-exponential factors calculated from the temperature dependence of the nitrogen diffusivity in niobium and niobium nitrides, which was obtained by using concentration profile fitting and the forward finite difference simulation.

Concentration profile fitting

Phase	δ-NbN (high c)	δ-NbN (low c)
E [eV]	3.19±0.10	3.20±0.10
D_0 [cm^2/s]	$0.68\ ^{+0.59}_{-0.31}$	$1.10\ ^{+1.02}_{-0.53}$

Forward finite differences

Phase	δ-NbN_{1-x}	β-Nb_2N	α-Nb(N)
E [eV]	3.32±0.03	4.0±0.1	2.44±0.04
D_0 [cm^2/s]	$2.2\ ^{+0.4}_{-0.3}$	$1.2\text{x}10^{2}\ ^{+1.7}_{-0.7}$	$1.8\text{x}10^{-1}\ ^{+0.6}_{-0.4}$

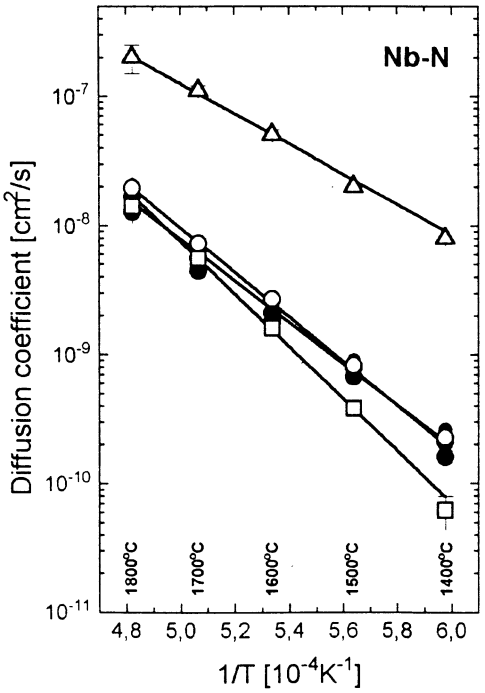

Figure 3: The nitrogen diffusion coefficients obtained from layer growth for α-Nb(N) (open triangles), β-Nb_2N (open squares) and δ-NbN (open circles). Diffusion coefficients calculated from the nitrogen concentration profiles in δ-NbN_{1-x} are plotted by solid circles.

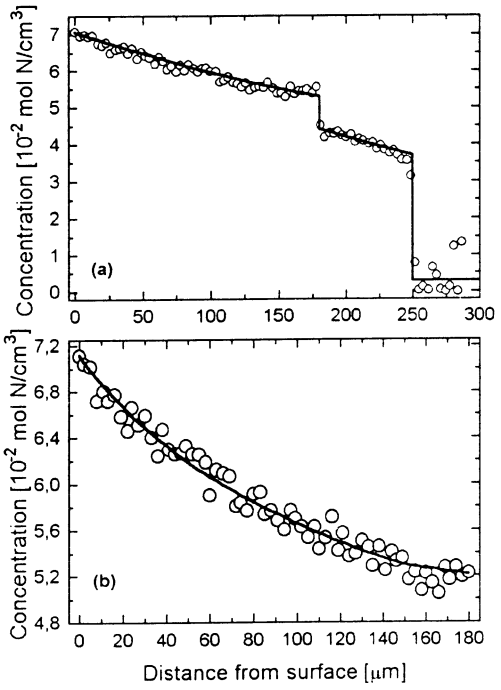

Figure 4: (a) the nitrogen concentration profile measured over δ-NbN_{1-x}, β-Nb_2N_{1-x} and α-Nb(N) (open circles) and simulated by the FFD method using concentration-independent diffusion coefficients (solid line). (b) the nitrogen concentration profile in δ-NbN_{1-x} (open circles) approximated by the function (9) assuming the diffusivity depends on the nitrogen concentration according to Eq. (10), solid line.

The diffusion coefficients of nitrogen in δ-NbN_{1-x} were found to be nearly independent of the nitrogen concentration, the first indicator of which was a good agreement between the measured concentration profiles and the concentration profiles simulated using the FFD method with concentration-independent diffusion coefficients (Fig. 4a). Note that upon the calculation of diffusion coefficients from the layer growth only the measured and the simulated positions of phase boundaries are compared, not the concentration profiles. The negligible concentration dependence of the nitrogen diffusion coefficient for δ-NbN_{1-x} was confirmed by the concentration profile fitting (Fig. 4b), which yielded a very low value of the parameter a in Eq. (10), $a = 20$ cm^3/mol.

4.2 Nb-C system

The Nb-C system was investigated between 1500°C and 2100°C [13]. Four phases are stable below 1570°C: α-Nb(C) (Im3m), β-Nb_2C ($P\bar{3}1m$), ζ-Nb_4C_3 ($R\bar{3}m$) and δ-NbC (Fm3m); above 1570°C, the ζ-Nb_4C_3 phase disappears. The homogeneity ranges measured using EPMA/WDS are shown as a part of the phase diagram in Fig. 5. The homogeneity range of ζ-Nb_4C_3 was measured using EPMA (40.1 – 40.7 at %) [11], thus this phase behaves as a line compound. Accordingly, the ζ-Nb_4C_3 phase was only observed in the Nb_2C/C diffusion couples but not in the Nb/C diffusion couples [14]. The reason is that the large concentration gradient and consequently the large diffusion flow in the Nb/C diffusion couples (in comparison with the Nb_2C/C diffusion couples) restricts the development of line compounds during the diffusion process [3]. Consequently, the ζ-Nb_4C_3 phase was not considered for calculation of the diffusion coefficients at 1500°C although it is thermodynamically stable at this temperature.

The carbon diffusion coefficients obtained from the layer growth for α-Nb(C), β-Nb_2C and δ-NbC are summarised in Fig. 6 (open symbols) and compared with the diffusion coefficients calculated from the carbon concentration profiles in δ-NbC_{1-x} (solid circles). The Arrhenius dependence of the diffusion coefficients yielded the activation energies and pre-exponential factors, which are given in Tab. 2. The activation energies given in the literature for the carbon diffusion in δ-NbC vary among 3.21 eV [15] and 4.02 eV [16] as studied by the layer growth or by weight gain, respectively.

The diffusion coefficients of carbon in δ-NbC_{1-x} were found to be strongly dependent on the carbon concentration; the differences in the diffusivity of carbon

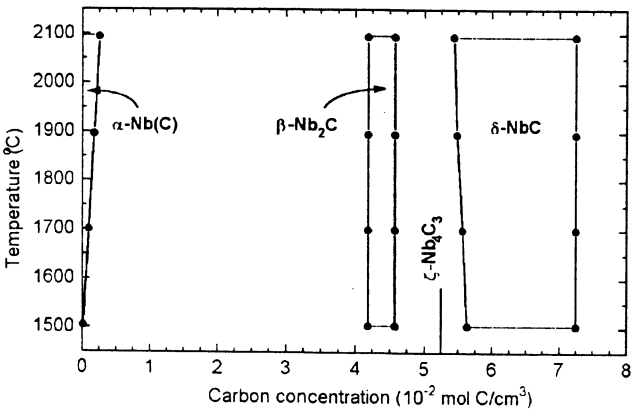

Figure 5: A part of the phase diagram for the Nb-C system. The circles indicate the limit concentrations used for calculation of diffusion coefficients from the layer growth. The ζ-Nb_4C_3 phase did not grow in the diffusion couples used for calculation of the diffusion coefficients.

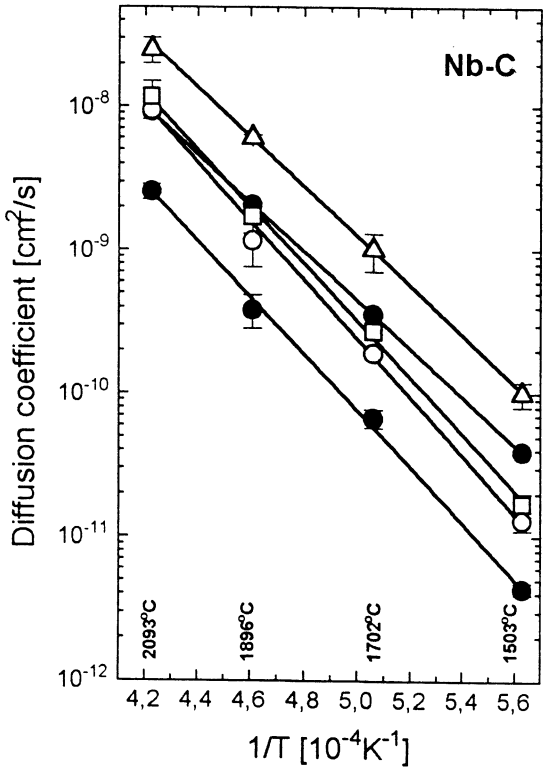

Figure 6: The carbon diffusion coefficients obtained from the layer growth for α-Nb(C) (open triangles), β-Nb_2C (open squares) and δ-NbC (open circles). Diffusion coefficients calculated from the carbon concentration profiles in δ-NbC_{1-x} are plotted by the solid circles. The higher diffusivities correspond to the respective minimum carbon concentration; the lower diffusivities are for the stoichiometric δ-NbC.

Table 2: Activation energies and pre-exponential factors calculated from the temperature dependence of the carbon diffusivity in niobium and niobium carbides, which was obtained using the concentration profile fitting and the forward finite difference simulation.

Concentration profile fitting

Phase	δ-NbC (high c)	δ-NbC (low c)
E [eV]	3.86±0.13	3.35±0.20
D_0[cm^2/s]	$0.4\ ^{+0.4}_{-0.2}$	$0.12\ ^{+0.4}_{-0.2}$

Forward finite differences

Phase	δ-NbC_{1-x}	β-Nb_2C	α-Nb(C)
E [eV]	3.97±0.14	3.95±0.10	3.40±0.10
D_0[cm^2/s]	$0.4\ ^{+0.4}_{-1.3}$	$2.9\ ^{+2.3}_{-1.3}$	$0.45\ ^{+0.13}_{-0.10}$

in the carbon-rich and in the carbon-poor δ-NbC_{1-x} are up to one order of magnitude. This was first indicated by a poor agreement between the measured concentration profiles and the concentration profiles simulated using the FFD method with concentration-independent diffusion coefficients (Fig. 7a) and proved by the concentration profile fitting (Fig. 7b), which yielded a=100 cm^3/mol.

4.3 Cr-N system

The Cr-N system was investigated between 1230°C and 1420°C using diffusion experiments carried out at 31 bar N_2 [17]. In this temperature range (and for this nitrogen pressure) three phases are stable: α-Cr(N) (Im3m) with a very low solubility of nitrogen in chromium, β-Cr_2N ($P\bar{3}1m$) and δ-CrN (Fm3m) [18]. The homogeneity ranges measured using EPMA/WDS are shown as a part of the phase diagram in Fig. 8. Because of the limited nitrogen pressure, the nitrogen-rich limit of δ-CrN_{1-x} was shifted to lower concentrations. As the nitrogen-poor boundary of δ-CrN_{1-x} in the phase diagram also shifts to lower concentrations, which is given by the thermodynamics of the Cr-N system, the mean nitrogen concentration in δ-CrN_{1-x} decreased with increasing temperature.

The nitrogen diffusion coefficients obtained from the layer growth in α-Cr(N), β-Cr_2N and δ-CrN are given in Fig. 9 (open symbols) and compared with the diffusion coefficients calculated from the nitrogen concentration profiles in δ-CrN_{1-x} and β-Cr_2N_{1-x} (solid symbols). The Arrhenius dependence of the diffusion coefficients yielded the activation energies and pre-exponential factors, which are given in Tab. 3. The nitrogen diffusivity in δ-CrN_{1-x} is strongly dependent on the nitrogen contents. The concentration gradient near the sample surface (at high nitrogen concentrations) is substantially higher than the concentration gradient inside of δ-CrN_{1-x} (at low nitrogen concentrations), which could not be approximated by the concentration profile calculated with a concentration-independent diffusion

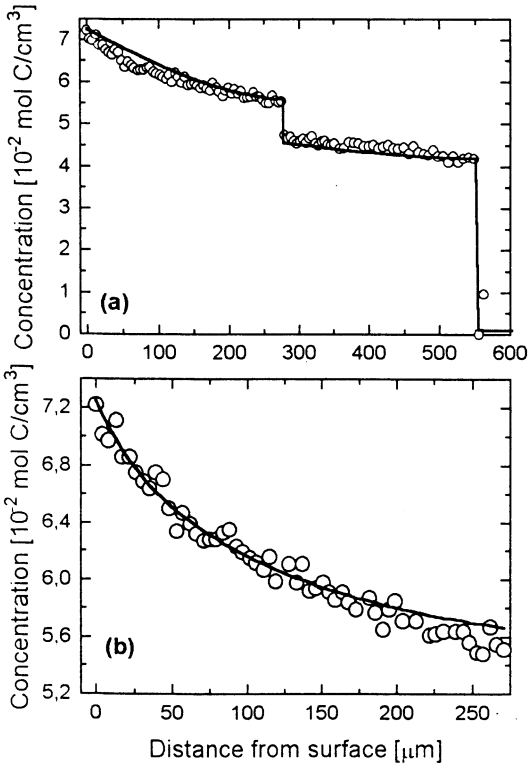

Figure 7: Comparison of the measured concentration profiles (open circles) with the concentration profiles calculated using the FFD method with the concentration-independent diffusion coefficients (a) and using the concentration profile fitting assuming the carbon diffusion coefficient in δ-NbC_{1-x} being exponential function of the carbon concentration (b).

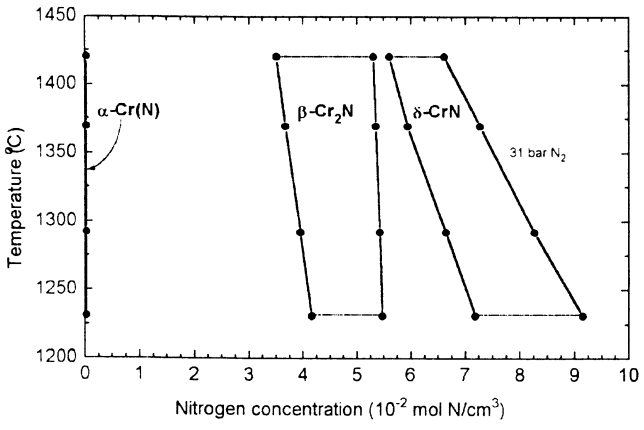

Figure 8: A part of the phase diagram for the Cr-N system. The circles indicate the limit concentrations used for calculation of diffusion coefficients from layer growth. The maximum nitrogen concentrations were reached with 31 bar N_2.

Table 3: Activation energies and pre-exponential factor determined from the temperature dependence of the concentration-independent (FFD simulation) and the concentration-dependent diffusion coefficient (calculated from the concentration profiles) in the Cr-N system.

Forward finite differencies

Phase	δ-CrN	β-Cr_2N	α-Cr(N)
E [eV]	5.12±0.08	2.68±0.15	2.79±0.15
D_0 [cm^2/s]	2.43x10^7	3.51	23.9

Concentration profile fitting

Phase	δ-$CrN_{1.00}$	δ-$CrN_{0.67}$
E [eV]	2.83±0.10	3.01±0.10
D_0 [cm^2/s]	9.21x10^{-3}	11.0

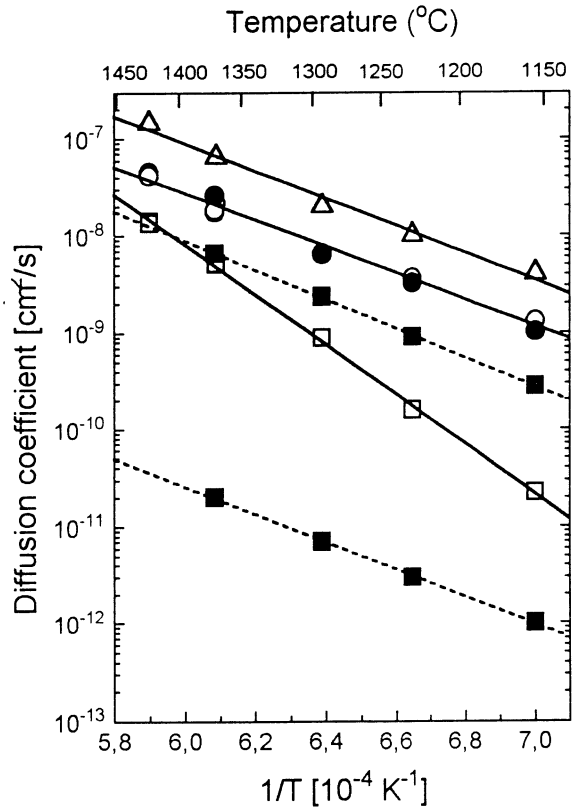

Figure 9: The concentration-independent diffusion coefficients of nitrogen obtained from layer growth in α-Cr(N) (open triangles), β-Cr_2N (open circles) and δ-CrN (open squares) are compared with the concentration-dependent diffusion coefficients calculated from the nitrogen concentration profiles in β-Cr_2N_{1-x} (solid circles). Solid squares denote the nitrogen diffusion coefficients in δ-$CrN_{0.67}$ (high diffusivity) and in δ-CrN (low diffusivity). These values were obtained by extrapolating the concentration-dependent diffusion coefficients calculated from concentration profiles to 40 at % N and 50 at % N, respectively.

coefficient (broken line in Fig. 10a). The nitrogen concentration profile was well approximated by the analytical function if the concentration-dependent diffusion coefficient was employed (solid line in Fig. 10a). The temperature and concentration dependence of the nitrogen diffusion coefficient in δ-CrN_{1-x} was described by the logarithmic surface (Fig. 11):

$$D\left[\mathrm{cm}^2/\mathrm{s}\right] = 0.018 \times \exp\left(-\frac{2.92\mathrm{eV}}{k_B T}\right) \times \exp\left(17.2x\right) \quad (12)$$

where x is the deviation from stoichiometry. The difference in the nitrogen diffusivities for δ-CrN and δ-$CrN_{0.67}$ is more than two orders of magnitude. Such a broad homogeneity range has not been reached for high temperatures because of the limited nitrogen pressure or is not present at low temperatures (see the phase diagram, Fig. 8). Nevertheless, the temperature shift in the mean nitrogen concentration together with the very strong concentration dependence of the nitrogen diffusion coefficient had an important consequence for the diffusion coefficients calculated from the layer growth. As the mean concentration decreased with increasing temperature, a steeper increase of the diffusion coefficient was found than it corresponds to its sole temperature dependence because the temperature dependence was overlapped by the concentration dependence of the diffusion coefficient in δ-CrN_{1-x} (Fig. 11). Regarding the low scatter in the measured concentrations, it was also possible to evaluate the nitrogen diffusion coefficients in β-Cr_2N from the concentration profiles. These diffusion coefficients agree well with those obtained from the layer growth, and the diffusion coefficients in β-Cr_2N were found to be independent of the nitrogen concentration (Fig. 10b).

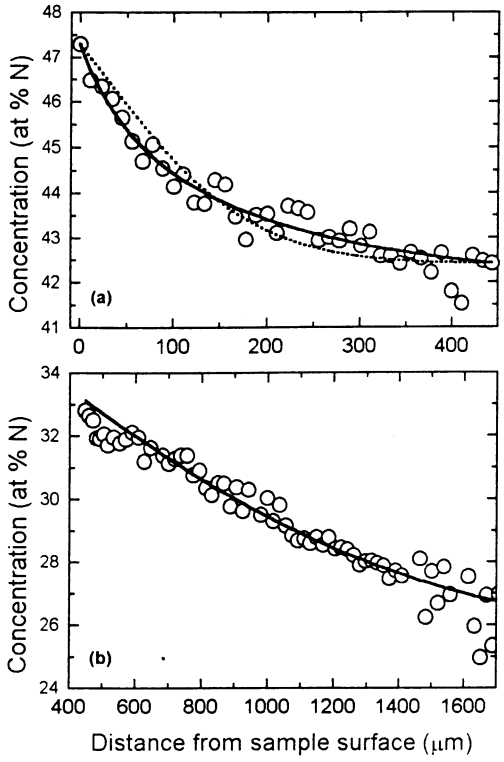

Figure 10: (a) the steep concentration gradient at the sample surface observed in δ-CrN_{1-x} is a typical indicator of the strong concentration dependence of the diffusion coefficient. Therefore, the concentration profile calculated with the concentration-independent diffusion coefficient (dotted line) cannot approximate the measured concentration profile (open circles). A good fit was obtained with the concentration-dependent diffusion coefficient. (b) no significant concentration dependence of the diffusion coefficient has been observed for β-Cr_2N_{1-x}, and therefore the concentration profile calculated with the concentration-independent diffusion coefficient approximates the measured concentrations well.

4.4 Cr-C system

The Cr-C system was investigated between 1260°C and 1410°C [17]. In this temperature range four phases having very narrow homogeneity ranges are stable: Cr(C) (Im3m), $Cr_{23}C_6$ (Fm3m), Cr_7C_3 (Pnma) and Cr_3C_2 (Pnma) [18]. The homogeneity ranges measured using EPMA/WDS are shown as a part of the phase diagram in Fig. 12. However, because of the narrow homogeneity ranges the measured concentration profiles (see Fig. 13) were not suitable for calculation of diffusion coefficients, and therefore the comparison of two independent sets of diffusion coefficients cannot be given here.

The concentration-independent diffusion coefficients obtained from the layer growth are summarised in Fig. 14. Their temperature dependence yielded the activation energies and pre-exponential factors, which are given in Tab. 4. As the measured concentration profiles could not be evaluated by the profile fitting, the concentration dependence of the diffusion coefficient could not be examined. Nevertheless, regarding the

Table 4: Activation energies and the pre-exponential factors in the Cr-C system calculated from the concentration-independent diffusion coefficients, which were obtained from layer growth.

Phase	E [eV]	D_0 [cm^2/s]
Cr_3C_2	2.5±0.6	1.21×10^{-2}
Cr_7C_3	2.9±0.2	0.718
$Cr_{23}C_6$	3.2±0.6	1.28
Cr(C)	2.9±0.3	1.54

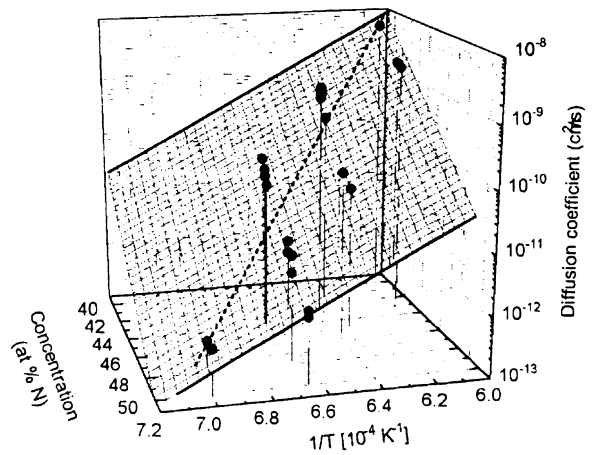

Figure 11: Logarithmic surface describing the temperature and concentration dependence of the nitrogen diffusion coefficient in δ-CrN_{1-x}. Solid circles are used for the diffusion coefficients obtained by the concentration profile fitting. The solid lines indicate the Arrhenius plots for δ-$CrN_{0.67}$ and δ-CrN, respectively. The broken line represents the oblique cut through different mean concentrations, which corresponds to the false Arrhenius plot for diffusion coefficients in δ-CrN_{1-x} obtained from layer growth (compare Fig. 9).

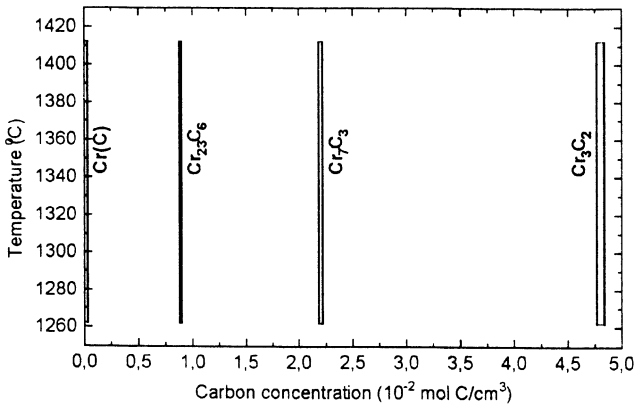

Figure 12: A part of the phase diagram for the Cr-C system used for calculation of diffusion coefficients from layer growth.

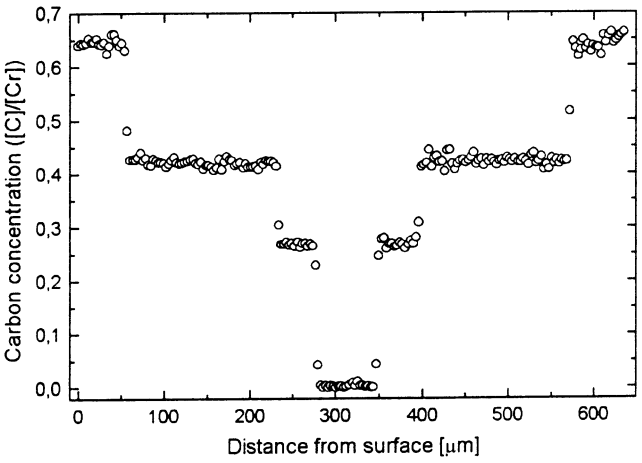

Figure 13: A typical carbon concentration profile in the Cr-C diffusion couple.

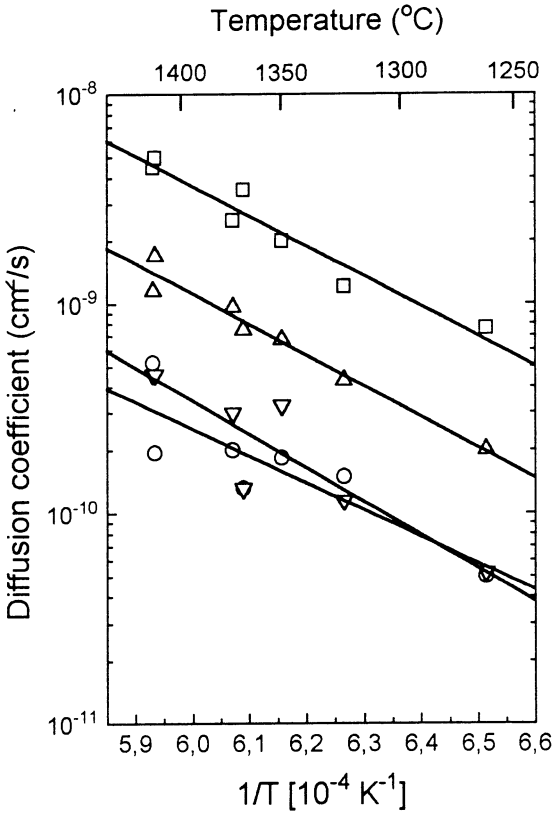

Figure 14: Concentration-independent diffusion coefficients of carbon in Cr(C)(open square), $Cr_{23}C_6$ (∇), Cr_7C_3 ($\triangle$) and Cr_3C_2 (o) as obtained from the layer growth.

narrow homogeneity ranges the diffusion coefficients can be assumed to be independent of the carbon concentration. The relatively high scattering in the carbon diffusion coefficients is caused partly by different porosity of the sample surface arising during the reactive diffusion, partly by the lower precision of diffusion coefficients calculated in phases with a narrow homogeneity range. The sample surface porosity influences especially the diffusion coefficients in the carbon-rich phases, Cr_3C_2 and Cr_7C_3, where the largest fluctuations of the diffusion coefficients were observed. The narrow homogeneity ranges imply a low concentration gradient inside the individual phases, which implies a low diffusion flow again. In such a case, the calculated positions of the phase boundaries are less sensitive to the changes of the diffusion coefficients. Thus a good match in the calculated and observed phase boundary positions was obtained upon a lower precision in the diffusion coefficients. The consequence is a higher fluctuation of the diffusion coefficients calculated from the layer growth.

Additional errors in the diffusion coefficients calculated from the layer growth are due to the limited accuracy of the homogeneity range measurement. According to Eqs. (5) and (7), the accuracy of both, the widths of the homogeneity ranges of individual phases and the widths of the two-phase regions, influences the precision of the calculated diffusion coefficients. This is striking in line compounds (phases with a very narrow homogeneity range), where the relative error in the homogeneity range width is larger than in the phases with a broad homogeneity range. Nevertheless, as the homogeneity ranges in the Cr-C system remain the same in the investigated temperature region, the inaccuracy of the concentration measurement might cause only a temperature-independent shift of diffusion coefficients in the Arrhenius plot that does not affect the obtained activation energies, but only the pre-exponential factors.

4.5 Ta-N system

The Ta-N system was investigated in the temperature range 1800°C – 1960°C [14]. Below 1860°C, four phases are stable: the α-Ta(N) solid solution of nitrogen in tantalum (Im3m), the intermediate β-Ta_2N phase ($P\bar{3}1m$), the δ-TaN_{1-x} phase (Fm3m) and the stoichiometric ϵ-TaN ($P6_3/mmc$). Below 1860°C, in equilibrium with ϵ-TaN the homogeneity range of δ-TaN_{1-x} is very narrow; the ϵ-TaN phase grows as a line compound. Above 1860°C, ϵ-TaN is not stable, and the homogeneity range of δ-TaN_{1-x} becomes broader. The maximum nitrogen concentration in δ-TaN_{1-x} depends strongly on the partial nitrogen pressure. The homogeneity ranges measured using EPMA/WDS are shown as a part of the phase diagram in Fig. 15, where also the influence of the nitrogen pressure on the maximum nitrogen concentration in δ-TaN_{1-x} is illustrated. Diffusion experiments at the lower temperatures were performed with the nitrogen pressure of 25 bar, the diffusion process at 1955°C was investigated at 10 bar N_2.

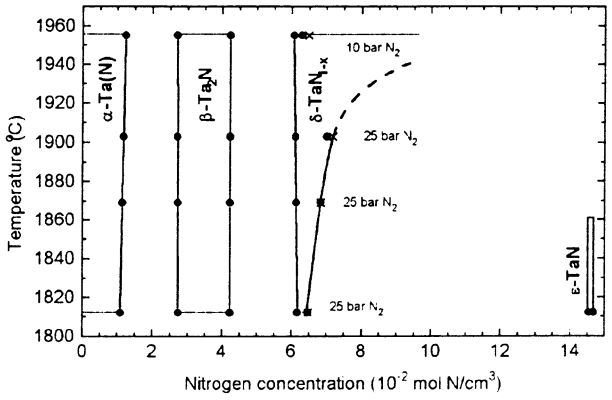

Figure 15: A part of the phase diagram for the Ta-N system. The measured limit concentrations are labelled by solid circles, the refined concentrations by crosses. Up to 1903° C, the maximum nitrogen concentration corresponds to 25 bar N_2; the diffusion experiment at 1955° C was performed with 10 bar N_2.

The concentration-independent diffusion coefficients obtained from the layer growth are given in Fig. 16 (large open symbols). Within β-Ta_2N_{1-x}, the diffusion coefficients were additionally calculated from the measured concentration profiles (solid triangles). The concentration profile fitting yielded the nitrogen diffusivity in β-Ta_2N_{1-x} being independent of the nitrogen contents. Moreover, the diffusion coefficients obtained from the layer growth and from the concentration profile fitting were completely matched. Therefore, the nitrogen diffusion coefficients for β-Ta_2N_{1-x} can be regarded as determined very precisely as they were obtained using independent approaches.

On the contrary, the diffusion coefficients for δ-TaN_{1-x} showed a strong deviation from the expected linear dependence in the Arrhenius plot. We believe that the reason is a low accuracy of the maximum nitrogen concentration in δ-TaN_{1-x} measured using EPMA/WDS in the samples prepared at the highest temperatures. This hypothesis was supported by inspecting Eqs. (5) and (7). As the maximum and the minimum concentrations and the diffusion coefficients occur as a product in these equations, they are strongly correlating and therefore a systematic error in one of them is deceptively corrected by deprecating the quality of the other. Thus, the surface nitrogen concentration was refined to linearise the Arrhenius plot for the δ-TaN_{1-x} phase. The refined maximum nitrogen concentrations are plotted by crosses in Fig. 15, the corresponding diffusion coefficients by small open squares in Fig. 16. The activation energies and the pre-exponential factors are given in Tab. 5.

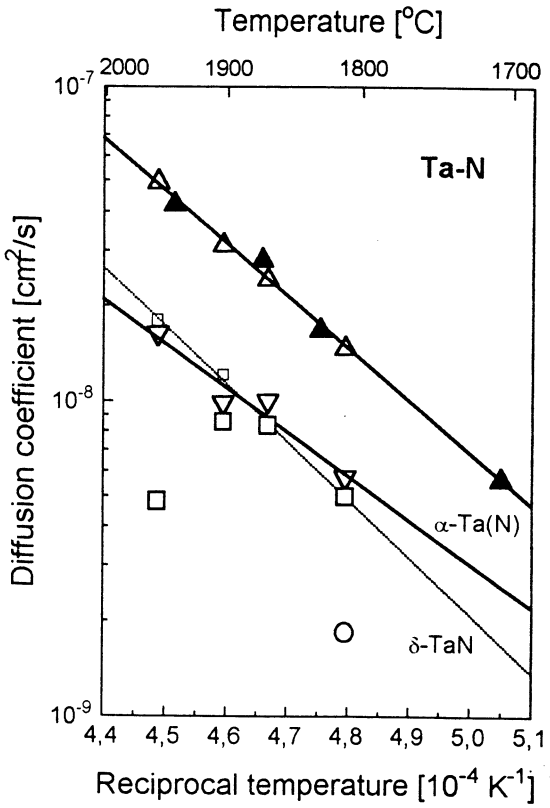

Figure 16: The concentration-independent diffusion coefficients of nitrogen in α-Ta(N) (open turned triangles), β-Ta_2N_{1-x} (open triangles), δ-TaN_{1-x} (open squares) and ϵ-TaN (open circle) as obtained from the layer growth. Large open squares denote diffusion coefficients calculated with the "as measured" limit concentrations; small open squares are the diffusion coefficients calculated with the refined limit concentrations. The diffusion coefficients in β-Ta_2N_{1-x}, which were obtained from the concentration profile fitting, are plotted by solid triangles.

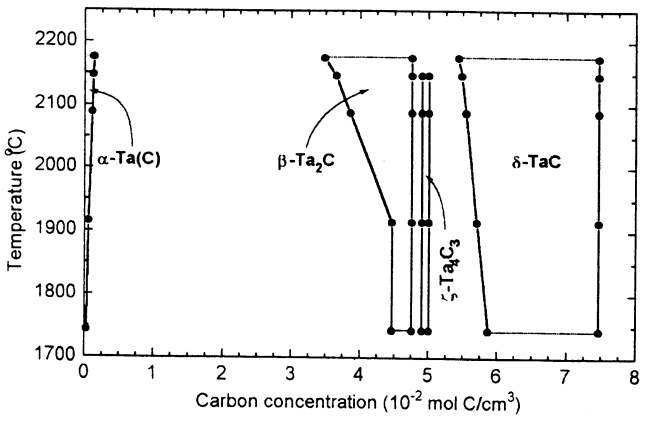

Figure 17: A part of the phase diagram for the Ta-C system. The circles indicate the limit concentrations used for the calculation of diffusion coefficients from the layer growth.

Table 5: Activation energies and pre-exponential factors for the nitrogen diffusion in tantalum and tantalum nitrides calculated from the diffusion coefficients obtained from the layer growth. In β-Ta_2N_{1-x} also the diffusion coefficients obtained from the profile fitting were taken into calculation.

Phase	E [eV]	D_0 [cm^2/s]
δ-TaN_{1-x}	3.6±0.1	$3.4\ ^{+3.5}_{-1.7}$
β-Ta_2N_{1-x}	3.30±0.09	$1.4\ ^{+0.9}_{-0.6}$
α-Ta(N)	2.8±0.5	$0.03\ ^{+0.40}_{-0.02}$

Upon measurement of the non-metal concentration profiles using EPMA, the edge of the sample and consequently the highest non-metal concentration is not well accessible in many cases. In addition, the concentrations measured near the edge are often affected by polishing effects [11]. Nevertheless, the surface concentration can frequently be obtained from the extrapolation of the measured concentration profile. This approach, however, failed for δ-TaN_{1-x} as it was discovered when calculating the activation energies. Thus, it can be assumed that the nitrogen concentration decreases very fast at the sample surface (as observed from the sample surface toward the centre). This is associated with a steep increase of the concentration gradient toward the sample surface, which is an indicator for the strong concentration dependence of the diffusion coefficient (see Cr-N). Unfortunately, as the concentration profiles in δ-TaN_{1-x} were not suitable for calculation of diffusion coefficients, this hypothesis has not been verified yet.

4.6 Ta-C system

The Ta-C system was investigated between 1700°C and 2200°C [14]. Below 2160°C, four phases are stable: α-Ta(C) (Im3m), β-Ta_2C ($P6_3/mmc$ up to approximately 2020°C and $P\bar{3}m1$ above 2020°C), ζ-Ta_4C_3 ($R\bar{3}m$) and δ-TaC_{1-x} (Fm3m). The ζ-Ta_4C_3 phase does not grow above 2160°C. The homogeneity ranges measured using EPMA/WDS are shown as a part of the phase diagram in Fig. 17. The carbon diffusion coefficients obtained from layer growth are shown in Fig. 18 (open symbols) and compared with the diffusion coefficients calculated from the carbon concentration profiles taken in δ-TaC_{1-x} (solid squares). In several samples, high-quality concentration profiles have also been measured in the β-Ta_2C phase, and therefore it was possible to obtain the independent set of diffusion coefficients for β-Ta_2C as well (solid triangles).

Whereas no significant dependence of the diffusion coefficient on the carbon concentration was found for the β-Ta_2C phase, the differences in the carbon diffusivity for the non-stoichiometric δ-$TaC_{0.77}$ and stoichiometric δ-TaC are nearly one order of magnitude. The temperature and concentration dependence of the dif-

Table 6: Activation energies and pre-exponential factors for the carbon diffusion in tantalum and tantalum carbides calculated from the diffusion coefficients obtained from the layer growth. In β-Ta_2C_{1-x} the activation energy and the pre-exponential factor were calculated from diffusion coefficients as obtained both from the layer growth enhacement (FFD simulation) and the concentration profile fitting.

	Forward finite differencies	
Phase	E [eV]	D_0 [cm^2/s]
δ-TaC_{1-x}	4.2±0.2	$1.1\ ^{+2.8}_{-0.8}$
ζ-Ta_4C_{3-x}	5.0±0.1	$20\ ^{+11}_{-7}$
β-Ta_2C_{1-x}	6.5±0.3	$1.1\text{x}10^5\ ^{+4.2}_{-0.9}$
α-Ta(C)	3.9±0.2	$4.2\ ^{+6.1}_{-2.5}$
	Concentration profile fitting	
δ-TaC	3.6±0.1	$0.023\ ^{+0.016}_{-0.009}$
δ-$TaC_{0.77}$	3.6±0.2	$0.14\ ^{+0.25}_{-0.09}$

fusion coefficient can be expressed by the exponential surface:

$$D(T,c) = (0.023 \pm 0.010)\,\mathrm{cm^2 s^{-1}} \times \exp\left[-\frac{(3.6 \pm 0.1)\,\mathrm{eV}}{k_B T}\right] \times \exp\left[(105 \pm 2)\,\mathrm{cm^3 mol^{-1}} \times (c^+ - c)\right] \quad (13)$$

with c^+ = 0.0747 mol C/cm^3, which is the concentration of carbon in the stoichiometric δ-TaC. The concentration dependence of the diffusion coefficient for δ-TaC_{1-x} is comparable with that for δ-NbC_{1-x}. Further activation energies and pre-exponential factors are given in Tab. 6.

Similar to the δ-CrN_{1-x} phase, different activation energies were obtained either from the layer growth or from the concentration profile fitting for δ-TaC_{1-x}. The reason is the same in both cases – the concentration-independent diffusion coefficient calculated from the layer growth is related to different average concentrations at different temperatures as the homogeneity range changes. This phenomenon is, of course, more striking for δ-CrN_{1-x} than for δ-TaC_{1-x} because the shift in the limit concentrations is larger in δ-CrN_{1-x}. Nevertheless, this result can explain some discrepancies found in the literature. Resnick et al [19] reported the activation energy for the carbon diffusion in δ-TaC of 3.7 eV as investigated by carburizing $TaC_{0.9}$ and by evaluating the measured concentration profiles. Nearly the same activation energy (3.64 eV) was given by Wakelkamp et al. [20] as a result of the diffusion couple technique (performed with the solid/solid diffusion couples). In both cases, the mean carbon concentration was kept constant, and therefore the activation energy corresponded to an iso-concentration cut in the exponential plane (Eq. 13). On the other hand, the activation energy given by Brizes [21] and Fromm et al. [22] was 3.9 eV and 4.3 eV, respectively. This was obtained from the layer growth in multiphase diffusion experiments, and therefore the activation energy was higher as it corresponds to the non-identical mean composition. These results agree perfectly with our findings (see Tab. 6).

5 Discussion

The diffusion kinetics was studied in relatively narrow temperature ranges. The choice of the appropriate temperature range was a compromise – the diffusion is a temperature-activated process, thus the non-metal diffusivity decreases exponentially with decreasing temperature, and the low temperatures imply very long diffusion times. Besides, the grain boundary diffusion, which can be neglected at high temperatures, becomes comparable with the bulk diffusion at low temperatures. The overlap of the grain boundary diffusion and the bulk diffusion would complicate the interpretation of the results.

Specific problems arising during the calculation of diffusion coefficients have been discussed above for individual materials. Besides, there are two common sources of errors in diffusion coefficients – inaccuracy in the concentration measurement and, investigating the layer growth, particularly the inaccuracy in reading the phase boundary positions. The inaccuracy in the concentration measurement affects both, the diffusion coefficients calculated from the layer growth and from the concentration profiles, but differently. Whereas large scatter in the measured concentrations or some artefacts in the concentration profiles due to the polishing effects are the principal difficulties upon the concentration profile fitting, the diffusion coefficients obtained from layer growth are mainly affected by the inaccurate maximum and minimum non-metal concentrations within individual phases (see δ-TaN, for example). Problems in the reading of the phase boundary positions arise if a phase decomposes upon cooling or if the phase band is very narrow. The very narrow layer thickness does also the concentration profile fitting impossible because of the limited lateral resolution of EPMA.

6 Conclusions

Two methods for calculation of the non-metal diffusion coefficients were presented and illustrated on the Nb-N, Nb-C, Cr-N, Cr-C, Ta-N and Ta-C systems. The first method employed the layer growth enhancement in the wedge-shaped diffusion couples; by using the second one the diffusion coefficients in individual phases were calculated directly from the shape of the concentration profiles. Whereas the investigation of the layer growth could be applied in all systems with known phase diagrams, the concentration profile fitting was applicable

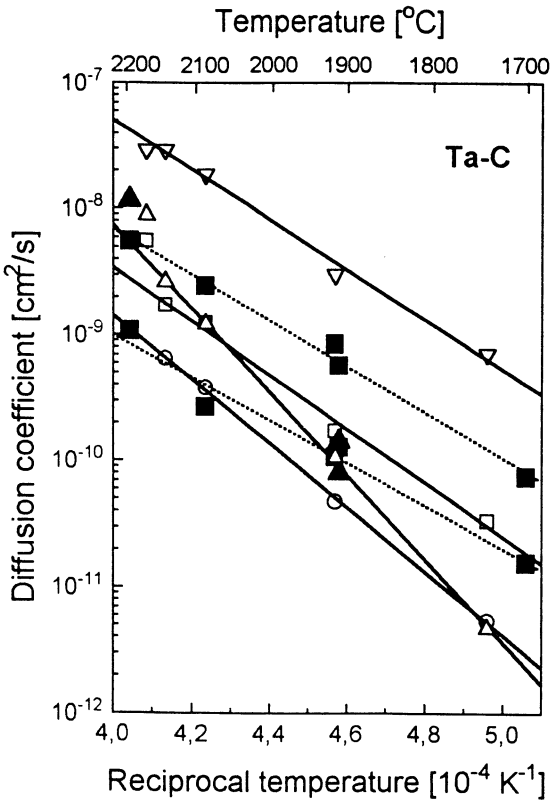

Figure 18: Diffusion coefficients of carbon in α-Ta(C) (turned triangles), β-Ta_2C_{1-x} (triangles), ζ-Ta_4C_{3-x} (circles) and δ-TaC_{1-x} (squares). Open symbols are used for the diffusion coefficients obtained from layer growth; solid symbols are for the diffusion coefficients calculated from concentration profiles.

only for non-metal-rich phases with a sufficiently broad homogeneity range, which excluded the solid solution of the respective non-metal in the host metal as well as the line compounds definitely.

On the contrary, the investigation of the layer growth enhancement yielded the concentration-independent diffusion coefficients, whereas the information on the concentration dependence of the diffusion coefficients could only be obtained by the concentration profile fitting. Therefore, the best way how to achieve the maximum information on diffusion coefficients was to compare the concentration-independent diffusion coefficients calculated from the layer growth with the concentration-dependent diffusion coefficients calculated from concentration profiles.

Acknowledgment

D. Rafaja would like to acknowledge the financial support of the "Lise-Meitner-Post-Doctoral-Research-Fellowship", No. M-00315-CHE through the Austrian "Fonds zur Förderung der Wissenschaftlichen Forschung".

References

1. W. Jost, Diffusion in Solids, Liquids and Gases, Academic Press Inc., New York, NY, 1960.
2. J. Philibert, Atom Movements, Diffusion and Mass Transport in Solids, Les Editions de Physique, Les Ulis, 1991.
3. N. Kidson, *J. Nucl. Mater.*, **3** (1961) 21.
4. D. Rafaja, W. Lengauer and P. Ettmayer, *Acta mater.*, **44** (12)(1996) 4835.
5. W. Lengauer, D. Rafaja, R. Täubler, C. Kral and P. Ettmayer, *Acta metall. mater.*, **41** (1993) 3505.
6. D. Rafaja and W. Lengauer, *Modelling and Simul. Mater. Sci. Eng.*, in press.
7. J. Crank, The Mathematics of Diffusion, 2nd edition. Oxford University Press, Oxford, U.K. (1987).
8. D. Rafaja, W. Lengauer, H. Wiesenberger and M. Joguet, *Metall. Mater. Trans. A*, in press.
9. F.J.J. van Loo and G.F. Bastin, *Metall. Trans.*, **A 20** (1989) 403.
10. M. Joguet, W. Lengauer, J. Bauer and M. Bohn, *J. Alloys Comp.*, in press.
11. W. Lengauer, J. Bauer, M. Bohn, H. Wiesenberger and P. Ettmayer, *Mikrochim. Acta*, **126** (1997) 279.
12. R. Musenich, P. Fabbricatore, G. Gemme, R. Parodi, M. Viviani, B. Zhang, V. Buscaglia and C. Bottino, *J. Alloys Comp.*, **209** (1994) 319.
13. H. Wiesenberger, W. Lengauer and P. Ettmayer, *Acta mater.*, in press.
14. H. Wiesenberger: PhD Thesis, Vienna University of Technology, 1995.
15. J. Fujikawa, P. Son, M. Miyake and T. Sano, *Japan Inst. of Metals*, **34** (1960) 1259.
16. T.C. Wallace and D.P. Butt: Review of Diffusion and Vaporization of Group 4 and 5 transition metal carbides in: Transition Metal Carbides and Nitrides: Preparation, Properties and Reactivity, ed. S.T. Oyama, Blackie Academic & Professional, London (1996), p. 77-90.
17. W. Mayr, W. Lengauer, P. Ettmayer, D. Rafaja, J. Bauer and M. Bohn, *Defect and Diffusion Forum*, **143-147** (1997) 546.
18. W. Mayr, W. Lengauer, P. Ettmayer, D. Rafaja, J. Bauer and M. Bohn, *J. Phase Equil.*, submitted.
19. R. Resnick, R. Steinitz and L. Seigle, *Trans. AIME*, **233** (1965) 1915.
20. W.F. Wakelkamp, F.J.J. van Loo, B. Boelen, G.F. Bastin and R. Metselar, *Defects and Diffusion Forum* (1989) 1485.
21. W.F. Brizes, *J. Nucl. Mater.*, **26** (1968) 227.
22. E. Fromm, E. Gebhardt and U. Roy, *Z. Metallk.*, **57** (1966) 808.